GEOPHYSICAL RESEARCH LETTERS, VOL. 35, L11105, doi:10.1029/2008GL033580, 2008

Improved horizontal wind model HWM07 enables estimation of equatorial ionospheric electric fields from satellite magnetic measurements

Patrick Alken,[1,2] Stefan Maus,[2] John Emmert,[3] and Douglas P. Drob[3]

Received 7 February 2008; revised 29 April 2008; accepted 19 May 2008; published 13 June 2008.

[1] Horizontal neutral winds play an important role in low-latitude ionospheric E and F-region dynamics. In particular, the zonal winds have strong effects on the local structure of the low-latitude ionospheric current system. Accurate wind specification is therefore essential for modeling these currents. In order to investigate the retrieval of eastward electric fields from satellite-derived equatorial electrojet (EEJ) profiles, we consider a provisional Horizontal Wind Model (HWM07) and its implications for the meridional structure of the EEJ. We find that EEJ current profiles predicted using HWM07 agree better with CHAMP magnetometer-derived current profiles than EEJ profiles predicted using the older HWM93 model. The improved wind model opens exciting new possibilities of determining the day-side eastward electric field in the equatorial ionosphere from satellite magnetic field measurements. **Citation:** Alken, P., S. Maus, J. Emmert, and D. P. Drob (2008), Improved horizontal wind model HWM07 enables estimation of equatorial ionospheric electric fields from satellite magnetic measurements, *Geophys. Res. Lett.*, *35*, L11105, doi:10.1029/2008GL033580.

1. Introduction

[2] Horizontal neutral winds have a large effect on the equatorial electrojet and the low-latitude ionospheric current system. These effects have been studied theoretically by *Richmond* [1973] and *Fambitakoye and Mayaud* [1976] among others and many of these findings have been reviewed by *Forbes* [1981]. Horizontal winds have significant effects on local electric fields and currents in the equatorial electrojet, though these effects have been notoriously difficult to detect with ground based measurements [*Hysell et al.*, 2002]. Significant new insight can be gained from the CHAMP satellite.

[3] The equatorial electrojet (EEJ) is an intense eastward current which follows the magnetic dip equator in the ionospheric E-region on the day side. Tidal winds drive currents during the day which cause positive and negative charges to accumulate at the dawn and dusk terminators respectively along the magnetic equator. This results in an eastward electric field which ultimately drives the equatorial electrojet [*Heelis*, 2004]. New satellite measurements of the EEJ have become available since July 2000 from CHAMP satellite magnetic field data. CHAMP magnetic data has been inverted to obtain height integrated latitudinal current density profiles of the EEJ [*Lühr et al.*, 2004]. This inversion process results in high quality meridional current profiles spanning nearly 7 years, and over 30,000 equator crossings.

[4] In a previous paper, we inverted averaged CHAMP profiles using the solutions of the governing electrodynamic equations to recover information about the eastward electric field and the zonal winds [*Maus et al.*, 2007]. In solving these equations, we used the Horizontal Wind Model (HWM) HWM93 [*Hedin et al.*, 1996] as the zonal wind input and found good agreement with the CHAMP observed current profiles. However the agreement was not perfect in some local time sectors. During 10–11 LT, HWM93 leads to predicted eastward current minima which were offset by several degrees in latitude from the CHAMP observed minima. This indicated a problem in the HWM93 zonal wind velocity at higher altitudes, since it is the high altitude winds whose effects propagate down equipotential field lines to affect the EEJ current off the dip equator. Also, during the evening (17–18 LT) the HWM93 winds lead to highly inaccurate current predictions which has been traced back to the lack of evening observations in HWM93 [*Maus et al.*, 2007, Figure 3].

[5] In the present study, we repeat much of the analysis from *Maus et al.* [2007] using a provisional Horizontal Wind Model HWM07. Using methods from earlier studies [*Sugiura and Poros*, 1969; *Richmond*, 1973] we solve the governing differential equation with HWM07 wind inputs to produce a height integrated current density which can be compared with the CHAMP observations. Using a least squares procedure, the CHAMP profiles can be inverted to produce an estimate of the eastward electric field and a DC shift in the eastward current. The zero-level shift is required due to the difficulties of separating the EEJ signal from background fields caused by the solar quiet (Sq) and magnetospheric ring currents [*Lühr and Maus*, 2006]. Using the provisional HWM07 model, we find a significantly improved agreement between the predicted profiles and the observed CHAMP profiles.

[6] In Section 2 we describe the provisional HWM07 model. In Section 3, we discuss the CHAMP derived data used for this study. In Section 4, we outline our method of modeling height integrated EEJ current profiles. Finally, we present and discuss the results of the modeling and inversion in sections 5–6.

2. Horizontal Wind Model

[7] HWM07 represents a significant overhaul of HWM93, including major formulation changes and the incorporation

[1]Department of Physics, University of Colorado, Boulder, Colorado, USA.
[2]National Geophysical Data Center, NOAA, Boulder, Colorado, USA.
[3]Space Science Division, U.S. Naval Research Laboratory, Washington, D. C., USA.

0094-8276/08/2008GL033580$05.00

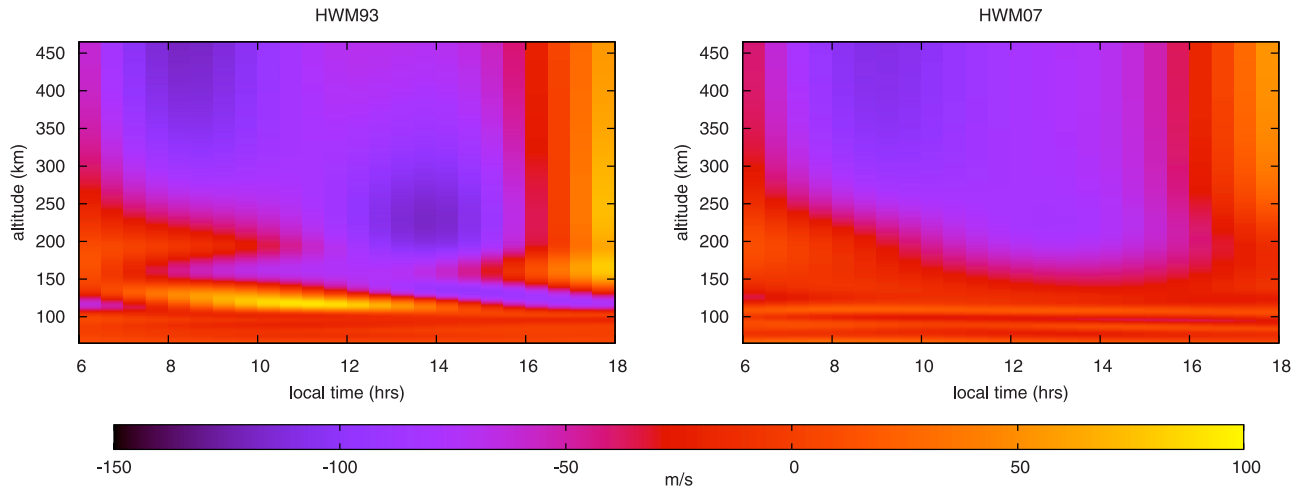

Figure 1. Average geographic eastward winds from (left) older HWM93 and (right) new HWM07 models for the altitude and local time ranges of interest.

of a substantial amount of new observational data. The model is still under development; complete details will be provided in a future publication, but a brief synopsis of the provisional version is provided here. The model is derived from extensive new ground-based and space-based wind measurements, including height profiles from NASA/UARS-WINDII and -HRDI instruments, height profiles from rocket-borne chemical releases, measurements from ground-based optical and radar instruments within the NSF-CEDAR database, lower atmospheric NOAA-NCEP data, and the data sets used in HWM93. In the thermosphere, the model consists of two empirical components: a quiet-time ($ap \leq 12$) component and a storm-time disturbance component (not used in this study).

[8] The quiet-time winds are represented by vector spherical harmonics (VSH) in geodetic latitude, geodetic longitude, and solar local time, up to wave numbers 8, 2, and 3, respectively. The seasonal dependence is represented by annual and semiannual Fourier harmonics. The vertical structure is represented by cubic B-splines with a node spacing of 5 km below 110 km, and higher nodes at 110,117, 125, 135, 150, 200, and 250 km. Above 250 km, the model winds asymptote to a constant value, with a relaxation scale height of 60 km; continuity up to the second derivative is imposed at 250 km. There is no solar cycle dependence in the provisional model; solar cycle effects are generally minor on the low latitude dayside [*Hedin et al.*, 1991], but the effect on nighttime winds can be significant [*Biondi et al.*, 1999].

[9] Importantly, a number of spurious artifacts in the HWM93 quite-time winds have been corrected, including the removal of a problematic derivative constraint at 200 km. The addition of WINDII profiles provided badly needed constraints on the model between 110 and 150 km, thereby removing an anomalous equatorial semidiurnal zonal wind oscillation in this region. HWM07 follows average WINDII profiles very closely in this region. In Figure 1 we show, as a function of local time and altitude, the zonal winds obtained from HWM93 and HWM07 along the dip equator, averaged over all longitudes and seasons. Particularly important for this study is the improvement in wind estimates in the evening near 100–150 km altitude.

3. CHAMP Observations

[10] The CHAMP satellite was launched in July 2000 into a near polar circular orbit with an initial altitude of 454 km. Its altitude has gradually decreased to about 350 km over the last 6 years. The satellite drifts slowly in local time, decreasing one hour every eleven days and completes an orbit every 92 minutes. The instruments used for this study are the scalar magnetometer which measures the field intensity, and the vector magnetometer whose orientation is determined by a dual-head star camera.

[11] The EEJ signature appears as a significant depression in the scalar magnetometer measurements of CHAMP. These measurements were then inverted for parallel line currents at 108 km altitude [*Lühr et al.*, 2004], with each line current representing a 0.5° wide band of height-integrated eastward current in corrected geomagnetic coordinates [*Richmond*, 1995]. There is some ambiguity in the background zero-level current due to difficulties in separating the background magnetic field. To overcome this ambiguity, independent inversions of the scalar and vector data were performed in order to validate a common zero-level. The independent inversions are in good agreement as shown by *Maus et al.* [2007, Figure 2]. Although inversions were completed for the vector data to validate the zero-level current, due to the more complete coverage of the scalar data, only these were used for the present investigation.

4. Computing EEJ Current Profiles

[12] The EEJ latitudinal current profiles as seen by CHAMP are primarily influenced by the E-region dynamo eastward electric field [*Heelis*, 2004], the conductivity, and the zonal winds [*Forbes*, 1981]. The equations

which govern the EEJ current are (in geocentric spherical coordinates):

$$\nabla \times \mathbf{E} = 0 \tag{1}$$

$$\mathbf{J} = \nabla \times \psi\hat{\boldsymbol{\phi}} + J_\phi\hat{\boldsymbol{\phi}} = \underline{\sigma}\left(\mathbf{E} + u_\phi\hat{\boldsymbol{\phi}} \times \mathbf{B}\right) \tag{2}$$

where $\mathbf{E}$ is the electric field, $\mathbf{J}$ is the current density, ψ is the stream function of the meridional current system, $\hat{\boldsymbol{\phi}}$ is a unit vector in the eastward direction, $\underline{\sigma}$ is the conductivity tensor [*Forbes*, 1981, equation (10)], u_ϕ is the eastward wind, and $\mathbf{B}$ is the ambient magnetic field. Once the stream function ψ is found, all other relevant fields and currents follow, as discussed by *Maus et al.* [2007]. The above equations can be formulated into a second order elliptic partial differential equation for the unknown stream function ψ [*Maus et al.*, 2007, equation (8)]. In the above equations, we ignore the effects of meridional winds as they have been shown to have a negligible contribution to the EEJ current [*Hysell et al.*, 2002]. Vertical wind effects are similar to an additional eastward electric field [*Forbes*, 1981], and it is certainly possible that they could have significant effects on the equatorial electrojet current [*Hysell et al.*, 2002]. However, due to the lack of data and reliable models we are unable to include their effects in this analysis.

[13] For boundary conditions, we demand that the stream function vanishes at the upper and lower boundaries and its normal derivative vanishes at the northern and southern boundaries. The PDE is then finite differenced on a 0.5° × 2 km mesh with an altitude range of 65 km to 465 km with a 9-cell stencil and solved using a sparse matrix algorithm. Once the stream function ψ is determined, the fields E_r and E_θ and the eastward current density J_ϕ follow from equations (3) and (5)–(7) [*Maus et al.*, 2007]:

$$\frac{\partial_\theta}{r\sin\theta}(\sin\theta\psi) = \sigma_{rr}E_r + \sigma_{r\theta}E_\theta + \sigma_{r\phi}E_\phi - \sigma_P B_\theta u_\phi \tag{3}$$

$$-\frac{\partial_r}{r}(r\psi) = \sigma_{\theta r}E_r + \sigma_{\theta\theta}E_\theta + \sigma_{\theta\phi}E_\phi + \sigma_P B_r u_\phi \tag{4}$$

$$E_\phi = \frac{RE_0}{r\sin\theta} \tag{5}$$

$$J_\phi = \sigma_{\phi r}E_r + \sigma_{\phi\theta}E_\theta + \sigma_{\phi\phi}E_\phi + \sigma_H|B|u_\phi \tag{6}$$

where σ_P and σ_H are the Pederson and Hall conductivities respectively, and E_0 is the equatorial eastward electric field at the reference radius R.

[14] To construct the conductivity tensor $\underline{\sigma}$, it is necessary to know the electron, ion and neutral densities and temperatures. This information is taken from the International Reference Ionosphere (IRI) [*Bilitza*, 2001] and the thermospheric model NRLMSISE-00 [*Picone et al.*, 2002]. While these models do not capture the full day-to-day variability of the ionosphere and thermosphere, they are believed to be quite accurate in the climatological mean, as needed for the present study. The magnetic field $\mathbf{B}$ is taken from the POMME-3 main field model [*Maus et al.*, 2006]. The zonal wind u_ϕ is taken from the Horizontal Wind Model [*Hedin et al.*, 1996]. Both HWM07 and the older HWM93 are used as inputs to compare the resulting current profiles. In a future study, we will use IRI and NRLMSISE-00 to model individual CHAMP passes and perform a more detailed analysis of their errors.

[15] *Maus et al.* [2007] allowed deviations from the HWM93 wind profile in order to obtain better fits to the observed CHAMP profiles. To reduce ambiguity, they imposed a constraint to keep these deviations as small as possible. Nevertheless, there is an ambiguity between the effect of an eastward electric field and a constant E-region zonal wind, making it difficult to simultaneously invert for both. Therefore, an improved zonal wind model would be very valuable in eliminating the need to optimize the wind solution, making it possible to invert only for the electric field and a zero-level current shift. In this study, we consider the effects of the new HWM07 model without any optimizations and compare the results to our previous study which allowed optimizations to HWM93.

[16] As described more fully by *Maus et al.* [2007], the HWM93 wind optimizations were done by solving the governing PDE for each of a set of cubic B-splines representing the true wind solution, resulting in a set of current profiles which can be linearly combined to fit the corresponding CHAMP profile, while simultaneously minimizing the difference between the optimized wind and HWM93. It is possible to linearly combine solutions of the PDE solved for separate wind profiles since the differential equation, as well as the wind and electric field terms, are linear. This makes it possible to treat winds at different altitudes separately in solving the PDE and linearly combining the solutions afterward. The B-spline knots were taken at 90, 100, 110, 120, 130, 140, 160, 190, and 240 km. Since it is difficult to simultaneously invert for both an electric field and a wind correction, due to inherent ambiguities, we imposed constant electric field values when solving for the optimized wind profiles. The electric field values used were taken from averaged JULIA radar data [*Hysell et al.*, 1997] and are given by *Maus et al.* [2007, Table 1].

[17] The error function used in the inversion process is given by

$$\chi^2 = \sum_i \left(J_i^{CHAMP} - J^{model}(\theta_i)\right)^2 + C_u \sum_j \left(u_j^{HWM} - u^{model}(r_j)\right)^2 \tag{7}$$

where J_i^{CHAMP} is the meridional EEJ current seen by CHAMP, $J^{model}(\theta_i)$ is the corresponding current solution from our modeling scheme, u_j^{HWM} is the zonal wind output from HWM, and $u^{model}(r_j)$ is the optimized wind for the HWM93 case. $C_u = 10^{-9}$ $(\mathbf{A} \cdot \mathbf{s}/\mathbf{m}^2)^2$ is the damping coefficient when optimizing the winds (HWM93), and $C_u = 0$ when not optimizing the winds (HWM07). The current model J^{model} is given by

$$J^{model} = J^{PDE}(E_0, u) - J_0 \tag{8}$$

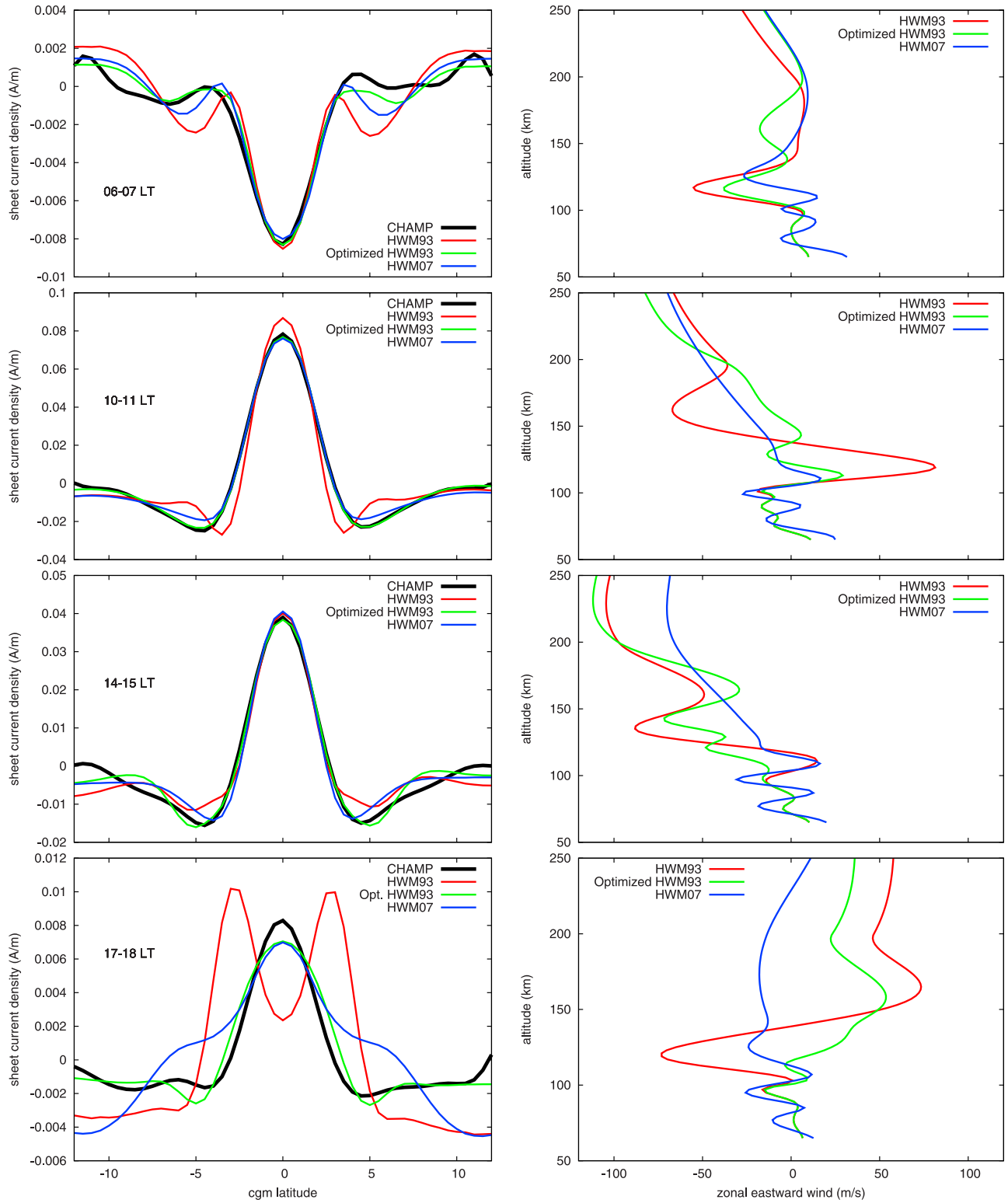

Figure 2. (left) Average CHAMP-derived current profiles as a function of corrected geomagnetic latitude (cgm) for four local time sectors; CHAMP observations in black, HWM93 solutions in red, optimized HWM93 solutions in green, and HWM07 solutions in blue. (right) Vertical wind profiles from HWM93 and HWM07 along with the optimized solution based on HWM93 in green.

where J^{PDE} is the height-integrated current solution derived from solving the governing PDE, J_0 is a constant zero-level shift, and E_0 is the electric field value to be optimized during inversion, initially taken as 1 mV/m. For the case of HWM93, u is a linear combination of B-splines with coefficients to be determined by the inversion, and for the case of HWM07, u is the wind output from that model, taken as is.

5. Results

[18] We analyzed averaged profiles in four local time sectors, though this technique could be applied to any individual satellite pass. We used input values of Kp = 2 and an F10.7 index of 120 for the IRI and NRLMSISE-00 models since they represent the mean values over the observation period of the CHAMP data. The resulting conductivities were then averaged over all seasons and longitudes. The magnetic field and zonal wind input values as a function of latitude were also averaged over all seasons and longitudes and the eastward component of the magnetic field was ignored. Similar to our previous study [*Maus et al.*, 2007] we used satellite profiles derived from CHAMP scalar data and averaged them over all longitudes and seasons to obtain profiles to invert with our modeling scheme.

[19] Figure 2 shows the average CHAMP profiles along with the solutions derived from the HWM93 and HWM07 models and the wind profiles themselves for four local time sectors, 06–07, 10–11, 14–15, and 17–18 LT. The average CHAMP profiles are shown in black. The solution derived from HWM93 without any optimization is shown in red; the solution derived from HWM07 is shown in blue. The solution derived from optimizing the HWM93 wind profile is shown in green. The actual wind profiles are shown on the right. Since we are trying to eliminate the need to optimize the winds, the HWM07 solutions are taken "as is" with no optimization performed. For the unoptimized HWM93 and HWM07 solutions, the inversion procedure optimizes only for the eastward electric field E_ϕ and the DC current offset J_0. For the optimized HWM93 solutions, we impose an averaged electric field inferred from JULIA 150 km radar echoes [*Hysell et al.*, 1997] as given by *Maus et al.* [2007, Table 1] and optimize for small deviations from HWM93 to obtain the best fit to the observed CHAMP profile. The JULIA electric fields are imposed in order to avoid ambiguities in simultaneously inverting for an electric field and a wind solution. Comparing the unoptimized HWM93 and HWM07 solutions in different local time sectors, we find that the electric field values derived using HWM07 are on the order of 30–70% higher than those derived using HWM93. These HWM07 derived electric field values lead to significant improvements in modeling the observed CHAMP current profiles as discussed below.

6. Discussion

[20] Zonal neutral winds have significant effects on low-latitude electrodynamics, as demonstrated by the CHAMP EEJ meridional current profiles. The Horizontal Wind Model (HWM) is an important step toward modeling these winds and their effects on the EEJ. In this study, we have numerically solved the PDE governing the EEJ current profiles in order to set up an inversion scheme for the CHAMP profiles. Since the modeling scheme requires a good model of the zonal winds, we have been able to provide some validation of HWM07.

[21] The provisional HWM07 model leads to better EEJ current predictions in all local time sectors, compared to the older HWM93 model. Especially significant is the location of the eastward current minima in the 10–11 LT sector. The HWM93 solution predicts the minima at ±3–4°, whereas the new HWM07 result correctly positions them at ±5°, the average location as seen by CHAMP [*Lühr et al.*, 2004]. HWM07 also provides better agreement with CHAMP for the 06–07 LT sector, which is during the (westward) counter-electrojet period. During the evening 17–18 LT sector there is also improvement. The older HWM93 model had a large westward wind around 100–150 km altitude which led to the incorrect double-peak structure in the corresponding current solution. With the addition of extensive UARS daytime lower and middle thermosphere wind profiles, HWM07 has largely corrected this feature, although it does not produce a complete agreement with the CHAMP current profile. One problem is that we could be close enough to the dusk terminator that the underlying simple current model may no longer be valid. In comparing the optimized HWM93 wind profiles to the HWM07 profiles, we find significant agreement in the first two local time sectors, especially at higher altitudes. In both the 06–07 LT and 10–11 LT sectors, the HWM07 profiles agree very well with the optimized HWM93 solutions which explains why the positions of the current minima in the HWM07 height-integrated current profile match much better with CHAMP, since these minima are affected by winds at higher altitudes. In the 14–15 LT sector the optimized HWM93 profile is much closer to the original HWM93 than the new HWM07 profile, but the current profile derived from HWM93 already agreed well with CHAMP and the new HWM07 current profile agrees even better. The optimized HWM93 wind solution must be taken with some caution because it is not unique. Finally, in the 17–18 LT sector, the HWM07 current profile is much improved over the double-peaked HWM93 profile though it does not give a good representation of the current minima.

[22] In this study we ignored the effects of meridional and vertical winds. Meridional winds have only a small contribution to the EEJ compared to zonal winds [*Hysell et al.*, 2002], and it is currently not possible to model vertical wind effects. Overall, we believe these results to be a positive validation of the use of HWM07 for obtaining electric fields from EEJ profiles.

[23] **Acknowledgments.** The operational support of the CHAMP mission by the German Aerospace Center (DLR) is gratefully acknowledged. The HWM development work was supported by NASA's Living with a Star Program and the Office of Naval Research.

References

Bilitza, D. (2001), International reference ionosphere 2000, *Radio Science*, *36*, 261–275.

Biondi, M. A., S. Y. Sazykin, B. G. Fejer, J. W. Meriwether, and C. G. Fesen (1999), Equatorial and low-latitude thermospheric winds: Measured quiet time variations with season and solar flux from 1980 to 1990, *J. Geophys. Res.*, *104*, 17,091–17,106.

Fambitakoye, O., and P. N. Mayaud (1976), The equatorial electrojet and regular daily variation S_R:-I. A determination of the equatorial electrojet parameters, *J. Atmos. Terr. Phys.*, *38*, 1–17.

Forbes, J. M. (1981), The equatorial electrojet, *Rev. Geophys.*, *19*, 469–504.

Hedin, A. E., et al. (1991), Revised global model of upper thermosphere winds using satellite and ground-based observations, *J. Geophys. Res.*, *96*, 7657–7688.

Hedin, A. E., et al. (1996), Empirical wind model for the upper, middle and lower atmosphere, *J. Atmos. Terr. Phys.*, *58*, 1421–1447.

Heelis, R. A. (2004), Electrodynamics in the low and middle latitude ionosphere: A tutorial, *J. Atmos. Sol. Terr. Phys.*, *66*, 825–838.

Hysell, D. L., M. F. Larsen, and R. F. Woodman (1997), Julia radar studies of electric fields in the equatorial electrojet, *Geophys. Res. Lett.*, *24*, 1687–1690.

Hysell, D. L., J. L. Chau, and C. G. Fesen (2002), Effects of large horizontal winds on the equatorial electrojet, *J. Geophys. Res.*, *107*(A8), 1214, doi:10.1029/2001JA000217.

Lühr, H., and S. Maus (2006), Direction observation of the F region dynamo currents and the spatial structure of the EEJ by CHAMP, *Geophys. Res. Lett.*, *33*, L24102, doi:10.1029/2006GL028374.

Lühr, H., S. Maus, and M. Rother (2004), Noon-time equatorial electrojet: Its spatial features as determined by the CHAMP satellite, *J. Geophys. Res.*, *109*, A01306, doi:10.1029/2002JA009656.

Maus, S., M. Rother, C. Stolle, W. Mai, S. Choi, H. Lühr, D. Cooke, and C. Roth (2006), Third generation of the Potsdam magnetic model of the earth (POMME), *Geochem. Geophys. Geosyst.*, *7*, Q07008, doi:10.1029/2006GC001269.

Maus, S., P. Alken, and H. Lühr (2007), Electric fields and zonal winds in the equatorial ionosphere inferred from CHAMP satellite magnetic measurements, *Geophys. Res. Lett.*, *34*, L23102, doi:10.1029/2007GL030859.

Picone, J. M., A. E. Hedin, D. P. Drob, and A. C. Aikin (2002), NRLMSISE-00 empirical model of the atmosphere: Statistical comparisons and scientific issues, *J. Geophys. Res.*, *107*(A12), 1468, doi:10.1029/2002JA009430.

Richmond, A. D. (1973), Equatorial electrojet - I. Development of a model including winds and electric field, *J. Atmos. Terr. Phys.*, *35*, 1083–1103.

Richmond, A. D. (1995), Ionospheric electrodynamics using magnetic apex coordinates, *J. Geomagn. Geoelectr.*, *47*, 191–212.

Sugiura, M., and D. J. Poros (1969), An improved model equatorial electrojet with a meridional current system, *J. Geophys. Res.*, *74*, 4025–4034.

P. Alken and S. Maus, National Geophysical Data Center, NOAA E/GC1, 325 Broadway, Boulder, CO 80305–3328, USA. (patrick.alken@noaa.gov)

D. P. Drob and J. Emmert, Space Science Division, U.S. Naval Research Laboratory, 4555 Overlook Avenue, S.W., Washington, DC 20375–5000, USA.